NANO LETTERS

Letter

pubs.acs.org/NanoLett

Room Temperature in Situ Growth of B/BO_x Nanowires and BO_x Nanotubes

Ignacio G. Gonzalez-Martinez,[†,‡] Sandeep M. Gorantla,[†] Alicja Bachmatiuk,[†,∥,⊥] Viktor Bezugly,[‡,§] Jiong Zhao,[†] Thomas Gemming,[†] Jens Kunstmann,[‡,#] Jürgen Eckert,[†,‡] Gianaurelio Cuniberti,[‡,§] and Mark H. Rümmeli*[,⊥,▽]

[†]IFW Dresden, Institute for Complex Materials, P.O. Box D-01171 Dresden, Germany

[‡]Technical University (TU) Dresden, Institute of Materials Science, D-01062 Dresden, Germany

[§]Max Bergmann Center of Biomaterials, TU Dresden, Budapester Strasse 27, D-01069 Dresden, Germany

[∥]Centre of Polymer and Carbon Materials, Polish Academy of Sciences, M. Curie-Sklodowskiej 34, Zabrze 41-819, Poland

[⊥]IBS Center for Integrated Nanostructure Physics, Institute for Basic Science (IBS), Daejon 305-701, Republic of Korea

[#]Department of Chemistry, Columbia University, 3000 Broadway, New York, New York 10027, United States

[▽]Department of Energy Science, Department of Physics, Sungkyunkwan University, Suwon 440-746, Republic of Korea

Supporting Information

ABSTRACT: Despite significant advances in the synthesis of nanostructures, our understanding of the growth mechanisms of nanowires and nanotubes grown from catalyst particles remains limited. In this study we demonstrate a straightforward route to grow coaxial amorphous B/BO_x nanowires and BO_x nanotubes using gold catalyst particles inside a transmission electron microscope at room temperature without the need of any specialized or expensive accessories. Exceedingly high growth rates (over 7 μm/min) are found for the coaxial nanowires, and this is attributed to the highly efficient diffusion of B species along the surface of a nanowire by electrostatic repulsion. On the other hand the O species are shown to be relevant to activate the gold catalysts, and this can occur through volatile O species. The technique could be further developed to study the growth of other nanostructures and holds promise for the room temperature growth of nanostructures as a whole.

KEYWORDS: *Nanowires, nanotechnology, room temperature, transmission electron microscope, electron beam damage, radiolysis, gold catalysis*

Boron nanowires have exciting properties which make them attractive for application in high-temperature ceramics, thermoelectrics, and lightweight armor.[1] To date, amorphous and crystalline boron nanowires (BNW) have been produced by magnetron sputtering,[2] chemical vapor deposition (CVD), and high-temperature laser ablation.[3−10] Crystalline boron nanowires can also be obtained by annealing amorphous nanowires.[7] Hybrid boron based nanowires are also possible. Xu and co-workers produced boron oxide coated boron nanowires and boron oxide nanotubes using CVD and Au catalyst particles.[11]

The synthesis of boron based nanostructures usually requires reaction temperatures well above room temperature, and in general, there still remains a lot to be understood on the growth processes of not only boron nanostructures, but nanostructures as a whole. This is because most synthesis approaches are ex situ and inherently provide indirect information. Thus, it is important to compliment ex situ studies with in situ studies. Transmission electron microscopy (TEM) is developing into a key in situ approach to investigate nanostructure growth. Usually this is achieved using specialized specimen holders that provide a heat source and gas supply[11−14] or a specialized holder with a heating element that resides in an environmental chamber in the objective lens where gas can be supplied.[15] In this work we demonstrate, for the first time, that one can grow nanowires in situ without the need of either an external gas supply or heating element. We employ Au nanoparticles that are catalytically active at room temperature.[16,17] In addition, we take advantage of electron beam−specimen interactions, in particular radiolysis to drive the reactions. In radiolysis electrons from the beam interact with the electrons from atoms in the specimen. This inelastic process can break chemical bonds and as such decompose material.

The initial material used as the precursor for our B/BO_x nanowires and BO_x nanotubes was first produced by a laser ablation process (see the Supporting Information).[18] At low magnifications (low electron dose) the amorphous BO_x matrix

Received: November 7, 2013
Revised: January 21, 2014
Published: January 27, 2014

ACS Publications © 2014 American Chemical Society

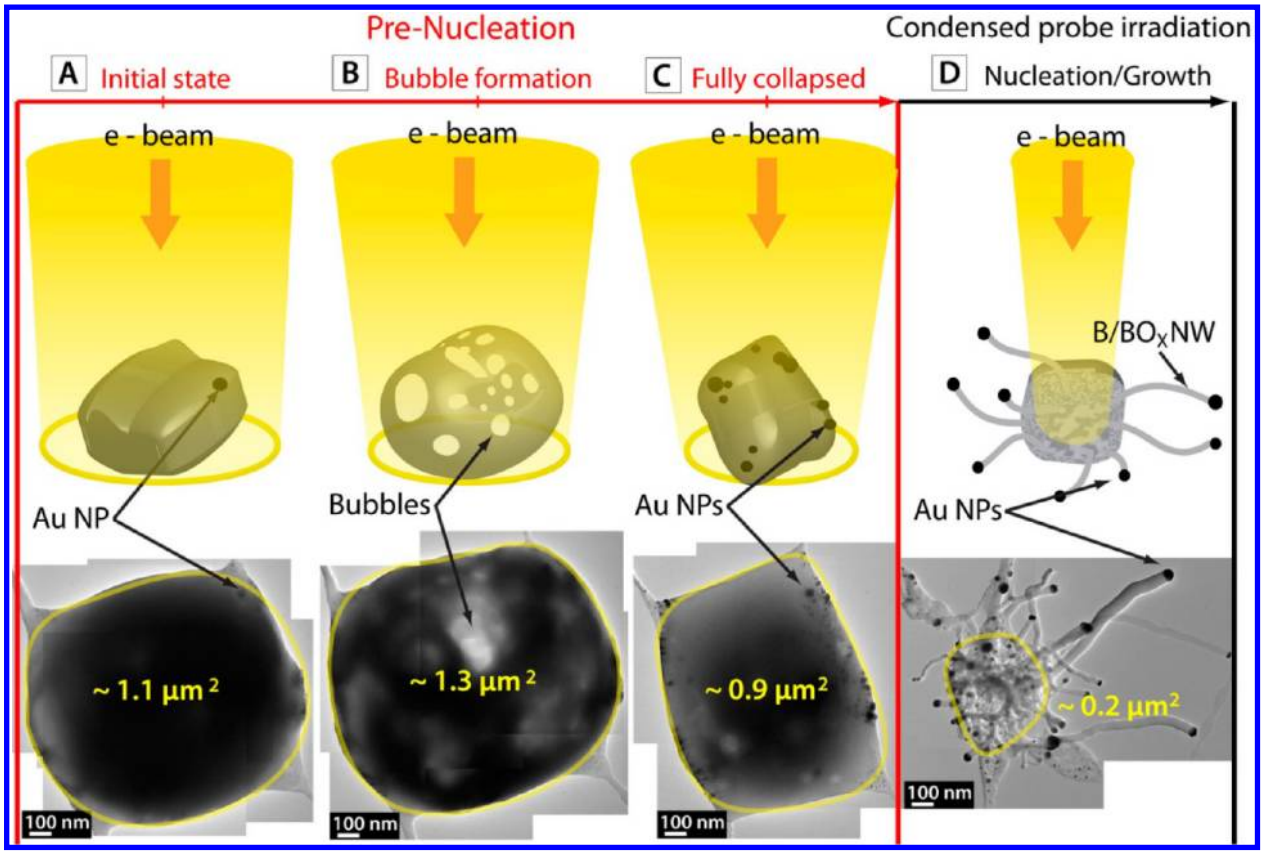

Figure 1. In situ synthesis steps. (A) The initial composite reacts mildly under a well-spread electron beam. As the beam waist is reduced (B) small bubbles start to form within the precursor composite due to radiolysis. The composite slightly inflates as indicated by the approximated area of the two-dimensional projection of the composite in the TEM image. (C) The composite collapses, and the Au nanoparticles are pushed toward the outer regions. (D) The nanowires are nucleated and continue to grow as long as a sufficiently high current density is provided. The growth process stops as the beam waist is once again enlarged, allowing us to obtain micrographs of the newly produced nanowires. A sizable loss in volume of the composite is now evident.

with embedded Au nanoparticles is relatively stable and can be imaged without any significant damage being observed as shown, for example, in Figure 1A. However, if one decreases the electron beam diameter (i.e., increase the electron dose), circular light regions form within the bulk precursor material, and the material is seen to slightly inflate. These regions are attributed to bubble formation (see Figure 1B). The more the beam diameter is decreased, the more rapid the bubble formation and eventual burst of the bubbles. Upon bursting the composite collapses reducing its volume in the process. As a consequence of the bubble collapse, many Au nanoparticles can be observed to move close to the composites surface (Figure 1C). If one squeezes the beam diameter yet further to ca. 4000 nm^2 (current density ca. 2.5×10^2 A/cm^2) and leaves this condensed beam resting for periods of 10 s, upon opening up the beam waist one observes that numerous nanowires now protrude from the composite. (Note: during compression of the beam, the camera shutter is closed to avoid damaging it; i.e., imaging only takes place with a broad beam diameter). Once the beam diameter is expanded, no growth of the fibers is observed; namely, growth only occurs with a highly condensed beam during which no direct observations outside of the irradiated region is possible. Figure 1D shows a typical example of the precursor matrix after nanowire growth. The volume of the composite is clearly reduced after the process since much of the material has been used to grow the new nanowires. Au nanoparticles are easily observed at the tips of the nanowires, suggesting they play a direct role in the nanowire growth. A closer examination of the nanowires shows they have a broad diameter distribution (5−100 nm). Typically, thin nanowires with diameters below 15 nm are somewhat "curly", while those with diameters above 40 nm are mostly straight. The diameters of the nanowires are uniform along their length and closely match that of the Au nanoparticle residing at their tip.

One can instigate further growth of the nanowires by condensing the electron beam again. Indeed, one can track their growth through successive cycles in which the electron beam is condensed and then spread (to monitor the nanowire growth). Figure 2A shows this process for growth times (condensed beam) of 5 s and then 10 s (see also Movie M1 in the Supporting Information). It can easily be seen that the increase in nanowire length is greater for the 10 s growth periods as compared to the 5 s growth periods. More detailed studies show that the growth rate with respect to the (total) irradiation time is only linear for only the first 30−40 s after which growth slows down dramatically or stops. This behavior is shown in the graph given in Figure 2A for two different nanowires. During the linear growth mode (short total irradiation time) the growth rates can exceed 7 μm/min. A closer inspection of the growth rates shows the growth rate tends to increase with increasing diameter (see Figure S2 in the Supporting Information). Moreover, during nanowire growth the composite is observed to get thinner and decrease in width due to

dx.doi.org/10.1021/nl404147r | Nano Lett. 2014, 14, 799−805

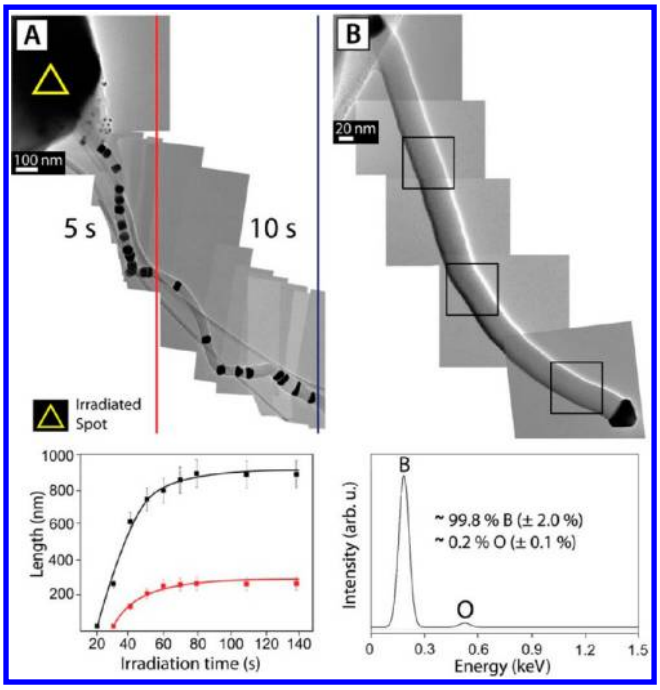

Figure 2. Growth tracking and chemical composition. (A) Superimposed frames tracking the growth of a single nanowire. The yellow triangle indicates the position and dimensions of the condensed electron beam as it irradiates the composite to instigate in situ nanowire growth. Each position of the Au NP corresponds to a single image. As can be deduced from the separation between consecutive Au catalyst positions, the growth rate is higher for irradiation periods of 10 s (between the red and blue lines) as compared to irradiation periods of 5 s (left side of the red line). The graph below shows the length of two different nanowires (black and red) as a function of the irradiation time. Although the black profile reaches a greater final length, the trend is analogous in both cases. (B) A typical EDS spectrum of a nanowire (note: the background has been subtracted). The relative atomic % of B and O are indicated in the inset. The figures stay constant along different sections along the nanowire (black boxes).

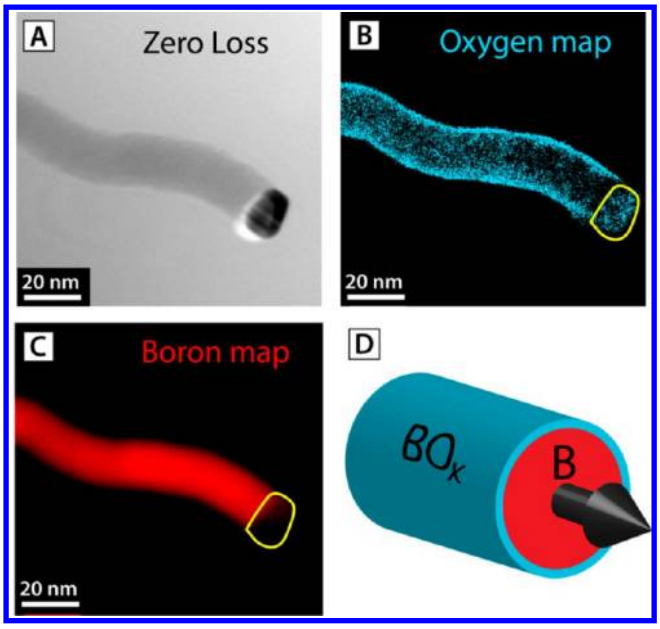

Figure 3. Zero loss and (false color) EFTEM images of a selected B/BO_x nanowire. B is uniformly distributed through the core, while O is found only at the surface. The elemental maps show a little presence of oxygen adsorbed on the Au tip (enclosed within the yellow curve), while B is absent. The schematic drawing shows the cross section of a nanowire highlighting its coaxial structure. The B core is shown in red, while the BO_x coating shell appears in light blue. The black arrow (panel D) points in the direction of the longitudinal axis.

material from the composite being used up to form the nanowires.

Energy dispersive spectra (EDS) taken from different sections along many nanowires consistently showed that their elemental composition is uniform along their length. The EDS data show they are primarily composed of B with only small traces of O (Panel B of Figure 2). Local electron energy loss spectroscopy (EELS) revealed that the relative B:O content is higher at the nanowire surface (Figure S3). Elemental B and O mappings of the nanowires using energy-filtered TEM (EFTEM), for example, Figure 3, confirmed that O is distributed along the nanowire surface, forming a thin oxide layer showing that wires are coaxial with a B core and BO_x shell.

We also observed that the Au nanoparticles at the tip of a growing wire undergo morphological changes during growth. The change in morphology can be easily observed when collecting images between condensed electron irradiation periods. Typically they go from having a smooth rounded shape to acquiring sharp facets and vice versa (these various aspects are shown in Figure S4). The morphological transitions were more frequent at short irradiation times ($\leq$100 s). In general, the smaller Au nanoparticles tend to change shape more often. Moreover, small variations in the width of the Au catalyst particle lead to small changes in the diameter of the growing fiber indicating a direct relationship between the catalyst diameter and that of the nanowire (see Figure S5 in the Supporting Information). In addition, no evidence hinting at a preferred orientation between the growth direction of the nanowires and the crystalline planes of the gold nanoparticles was found (see Figure S6 in the Supporting Information).

Uchiyama et al.[19] observed similar morphology changes of gold nanoparticles supported on CeO_2 at room temperature. The changes were attributed to changes in the partial pressure ratio of CO and O_2 and are not related to a reversible solid–liquid phase transition. In this study, irradiation of the composite provides a variable source of O_2. Oxygen desorption from the irradiated area was observed by EDS measurements taken during the condensed electron irradiation periods. The variations in the relative atomic percentage (at. %) B:O ratio were plotted as a function of the total irradiation time as for example shown in Figure 4A (alternative graphs focusing on the B and O at. % are shown in Figure S7). The B:O ratio tends asymptotically toward a saturation value which generally lies between 3 and 6 (15–25 O at. %). The initial steep increase in the B:O ratio trend shows that O is readily desorbed from the irradiated area during the early stages of irradiation. As the ratio B:O reaches a relatively stable value, the nanowires growth tends to slow down until growth either ceases or the catalyst particles moves inward forming a BO_x nanotube (discussed below). In cases where the nanowire stops growing, often it is possible to resume their growth simply by shifting the irradiation spot to another location over the composite (panels B and C of Figure 4). Nevertheless, at very long irradiation times ($\geq$500 s), the growth cannot be resumed by this means suggesting that the whole composite has become stable against electron irradiation.

As mentioned above, once the B:O ratio reaches a relatively stable value, sometimes, a BO_x nanotube starts to form. In this

dx.doi.org/10.1021/nl404147r | Nano Lett. 2014, 14, 799–805

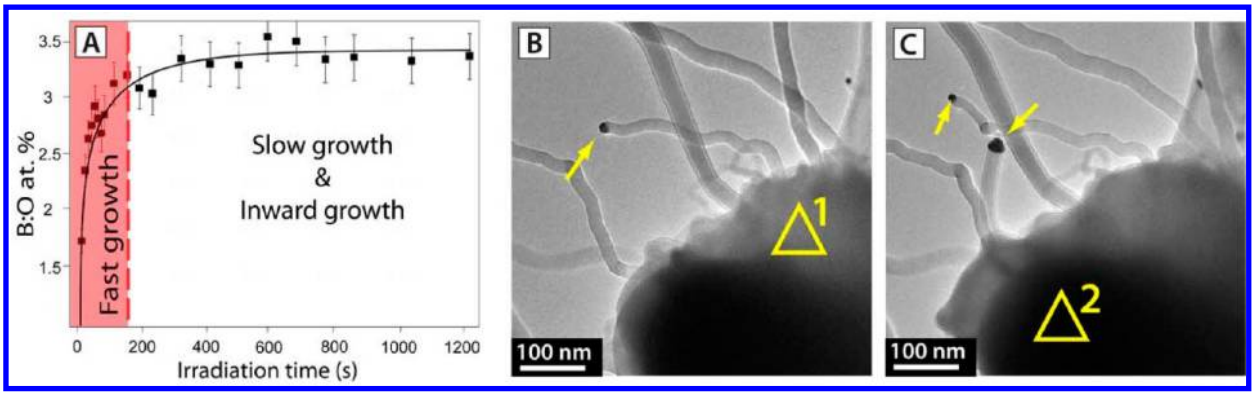

Figure 4. B:O (at. %) ratio variation and resumed nanowire growth. (A) Typical B:O (at. %) trend as a function of the total irradiation time, the approximate regions of fast growth and slow growth/inward growth are indicated. (B) After numerous irradiation periods at region 1 nanowire growth stops. (C) Growth can be resumed, and new nanowires nucleate by shifting the irradiation to a fresh region (region 2).

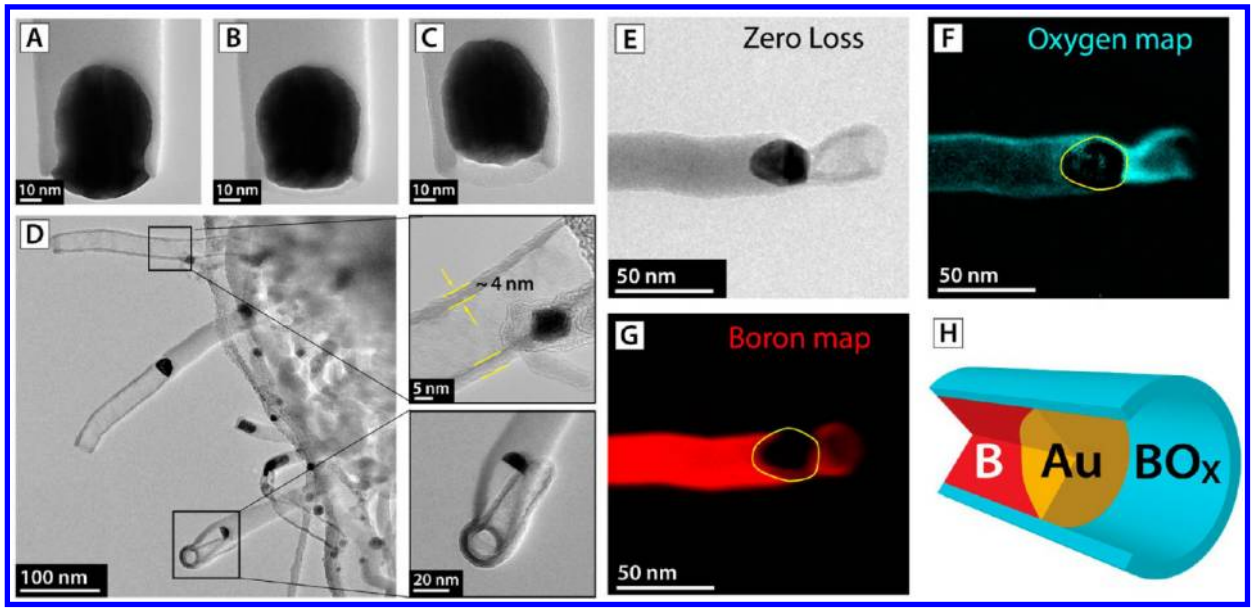

Figure 5. BO_x nanotube formation and zero loss and (false color) EFTEM images of a growing nanotube. (A–C) Au catalyst particle evolution at the onset of nanotube formation. The frames are taken after consecutive irradiation periods of 10 s. The gradual insertion of the Au nanoparticle into the nanowires core can be observed. (D) A group of long and regular BO_x nanotubes. The nanotube walls in the upper inset are clearly visible by their darker contrast. The bottom inset shows the remarkably circular cross section of one of the NTs. Panels E–H: The oxygen signal is clearly stronger in the tubular region indicating that the tube's walls are boron oxide. A schematic picture of the structure is shown in panel H.

process the Au catalyst particles move inward inside the nanowires and in the process removes the B core leaving only a BO_x shell, namely, a BO_x nanotube is formed as shown in Figure 5. The formation rates of the nanotubes are lower than those found for the nanowire growth (see Figure S8 in the Supporting Information). Again, as with the nanowire growth, all activity stops as soon as the beam is spread out. This suggests nanotube formation occurs only when both the B and O supply is limited. The composition of the nanotubes was initially checked by EDS. The measurements point to a higher relative O at. % in the tubular sections with respect to the filled regions of the nanowires concomitant with BO_x (Figure S9). EDS elemental mapping (300 kV electron irradiation) showed a higher relative O content in the tubular sections again suggesting the tubular sections comprise BO_x (Figure 5). In terms of the observed growth rates for the B/BO_x nanowires, they are 50 times higher than reported CVD growth rates for similar nanowires.[8] Moreover, given the in situ reaction takes place inside a TEM at high vacuum (ca. 10^{-7} mbar), it is hard to explain feedstock material being solely transported to the Au catalyst at the tip of a growing nanowire in gaseous form. Hence we devised a series of experiments to determine how the feedstock material is transported from the irradiated composite region to the Au catalyst particles at the tip of a tube. The data indicate B rich species are directly transported along the surface of a growing nanowire.

In the first experiment two nearby composites (ca. 300–500 nm) were located. We then alternately irradiated each of these composites to determine if simultaneous growth occurred from both composites. Growth was only ever observed for the irradiated composite. However, when nanowires from different composites come into direct contact, then irradiation supplied to either of the composites produces growth in both of the touching nanowires (Figure 6A). This result provides direct proof that the generated B species are not volatile, but instead they diffuse along the nanowire surface until they reach the Au tips to produce further growth.

dx.doi.org/10.1021/nl404147r | Nano Lett. 2014, 14, 799–805

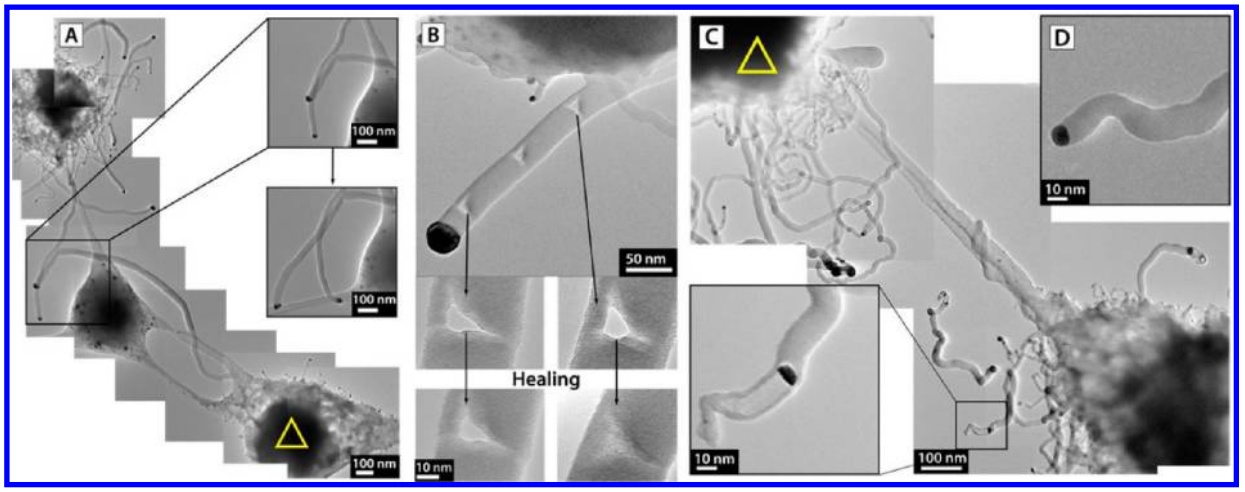

Figure 6. Neighbor composite experiments and hierarchical defect healing. (A) After the nanowires from different composites have made contact (upper inset), both can be made to grow by irradiating either of the composites (lower inset). (B) The holes in a drilled nanowire heal sequentially from base to tip as the total irradiation time progresses. (C) When the composite on the upper left corner is irradiated, the nanowires from the composite at the lower right corner are transformed into nanotubes as shown in the magnified box. (D) The same nanowire before inward growth is shown for comparison.

Table 1. Summary of Growth Parameters and Morphological Characteristics

	length (nm)	growth rates (nm/min)	atomic % B:O growth window	O atomic % growth window	diameter (nm)	wall thickness (nm)
B/BO_x NWs	1−4050	30 to >7000	2−6 (±0.5)	15−30 (±2)	<10 to >100	
BO_x NTs	1−610	105−350	3−6 (±0.5)	15−24 (±2)	10−60	2−5

In the second experiment three holes were drilled along a nanowire (Figure 6B). The holes were made by condensing the beam into a condensed probe and focusing it over a section of the nanowire for around 5 min. The probes size and shape match those of the holes. Then a spot on the composite near the base of the nanowire (with holes) was irradiated. Upon irradiation, the holes begin to fill with material in what can be thought of as a healing process. The filling of the holes occurs from the holes perimeter inwardly until it is fully covered. The healed hole does not fully recover to the initial thickness as indicated by a slightly lighter contrast. Moreover, the holes heal in a stepwise fashion, with the hole nearest the nanowire base (irradiation zone) healing first, and then the next nearest hole and so forth. Another defect healing process is provided in the Supporting Information in Figure S10. Again, these data point to the diffusion of feedstock material from the irradiation zone diffusing along the nanowire toward its free (Au) tip. In yet another experiment we again explored two nearby composites; however, this time both composites had nanowires stemming from them such that the distance between nanowire (Au) tips and the composite was below ca. 300 nm. In this configuration we found that sometimes, when irradiating one composite, a nanowire from the other composite (with no irradiation) would start to form a nanotube as shown in Figure 6C. This experiment confirms the importance of volatile oxygen species and limited B species for BO_x nanotube formation. In addition, given the forming boron nanotube is connected to a nonirradiated composite which is disconnected by the irradiated composite, it provides full proof that the process occurs at room temperature.

Table 1 provides an overview of some of the most relevant parameters describing the B/BO_x nanowires and BO_x nanotubes. In general, nanowire growth is significantly faster than nanotube formation. Nanotube formation tends to occur with a reduced oxygen presence. (A more graphical depiction of the growth regimes is shown in Figure S11).

We now turn to understanding the nucleation and growth mechanisms behind the nanowires and the nanotubes. During the early nucleation stages we observe the formation of bubbles all over the composite upon irradiation with an electron beams. The formation of bubbles has been observed before by Laval and Wesmacott[20] and De Natale and Howitt[21] who studied the formation of oxygen bubbles in silicate glasses under e-beam irradiation at moderate current densities. De Natale and Howitt attributed the oxygen evolution to a radiolytic chain reduction reaction taking place in the oxide groups that do not form part of the silica network. The reaction generates negatively charged oxygen species and positively charged metal ions. The oxygen recombines to produce O_2 molecules which can then form bubbles. They also showed how the radiolysis reaction can be generalized to any oxide. In our case for a B_xO_y molecule the reduction chain reaction can occur as:

$$2BO \rightarrow 2B^{+} + 2O^{-} \rightarrow 2B + O_2$$

The reaction is enhanced if there are large amounts of interstitially trapped oxygen in the specimen. This could account for the inflation and quick deflation which we observe when first irradiating a composite specimen. Once the composite has collapsed after releasing excess oxygen (bubble collapse), the major components of the irradiated area are B and O (trace impurities of Al, C, and Si are sometimes observed) and Au nanoparticles forming an amorphous composite, namely, amorphous B_xO_y embedded with Au nanoparticles. Other radiolysis reactions may also be at play. For instance, radiation induced oxygen desorption has been observed in B_2O_3 specimens bombarded with electrons.[22] In particular Auger spectroscopic studies of B_2O_3 leave open the possibility to generate O^0 and O^+ through interatomic Auger

dx.doi.org/10.1021/nl404147r | Nano Lett. 2014, 14, 799−805

processes as outlined by the Knotek–Feibelman (K–F) mechanism (Figure S12 in the Supporting Information).[22−24] In the K–F mechanism an O^+ cation finds itself within a local positive potential created by the neighboring metallic cations, after which it becomes dislocated or totally desorbed if it happens to be near the specimen's surface and has enough kinetic energy to escape. Indeed, this O^+ cation production process is a well-known radiolysis mechanism for oxides. Oxygen species generated deeper in the foil can recombine with trapped electrons (e.g., secondary's) to produce O_2 which ultimately also leaves the specimen. Such reduction reactions are known to occur, even at moderate current densities (10−50 A/cm^2)[25] and with sufficiently high current densities (4×10^3 to 2.5×10^4 A/cm^2) metal mono-oxide specimens can decomposed into a base metal and free oxygen.[26] Simultaneously, collective Auger emissions occurring in nonconductors like boron oxide (including those involved in the K–F mechanism) lead to a positive charging of the specimen (see Supporting Information). The charge build-up produces an internal electric field which can eventually disrupt the specimen. To compensate for the excess charge, positive ions (B^+ and possibly BO_x^+) are expelled laterally to re-establish electrostatic equilibrium.[27]

Thus, we postulate that, in our case, the K–F mechanism and substantial specimen charging as well as other radiolysis reactions lead to our boron oxide specimen being rapidly decomposed to yield various species (O^-, O^0, O^+, O_2, B^+, and BO_x^+). Some of these species will be volatilized and, at least for oxygen, play a critical role in activation of the Au catalysts. In addition, many species will diffuse along the surface (as experimentally confirmed). The positively charged species that constitute the feedstock material will be driven by electrostatic repulsion. This repulsive driving force can account for the incredibly high growth rates we observe. However, as the B and O supply deplete, continued growth at the (Au) tip of the nanowire depends on two factors, namely, sufficient oxygen to activate the Au catalytic process and second a supply of boron. If the supply of boron ceases or is sufficiently reduced, and so long as a small amount of oxygen is available to activate the Au nanoparticle, then the Au particle will start to use B from the nanowire releasing it into vacuum and in the process leave behind the boron oxide coating, thus forming a boron oxide nanotube. When the composite has been reduced sufficiently, first, insufficient oxygen to activate the Au nanoparticles will be produced, and second, the specimen will become conducting enough so that the charging effect is mitigated and thus no boron feedstock can be generated.

In terms of the temperature, the experimental data clearly point to room temperature growth; however, at nucleation where the Au nanoparticles and the BO_x composite are directly irradiated, temperature increases could occur. To investigate this we use a calculation route developed by Liu et al.[28] derived to determine the steady heat flow of thin films under electron bombardment (details are provided in the Supporting Information). For a specimen width of 500 nm we obtain a temperature rise of less than 10 K at the irradiated zone. To determine the temperature rise outside of the irradiated zone, we use a formula proposed by Egerton et al.[29] For a radial distance of 500 nm away from the irradiated (heated zone) we obtain a temperature rise of not more than 12 K. In terms of the Au catalyst particles heating under direct electron irradiation, we calculate their potential rise in a system embedded in boron oxide for Au (for an average Au particle size of radius equal to 20 nm). This yields a temperature rise of only around 10 K even after 1000 s of irradiation.[30] This points to increased temperatures not being important in either the nucleation or growth of the nanostructures; in essence, the process occurs at room temperature.

In summary, we demonstrate the feasibility of the catalytic growth of coaxial B/BO_x nanowires and BO_x nanotubes in situ in a TEM at room temperature. The entire process is driven by radiolysis reactions due to the irradiating electrons and so does not require an expensive specialized holder or TEM instrument for heating and gas injection. Remarkably high growth rates, some 50 times higher than observed in CVD growth, are observed for the amorphous coaxial B/BO_x nanowires, and this is attributed enhanced surface diffusion of charged B species due to electrostatic repulsion. Oxygen species are required to activate the Au catalyst nanoparticles, and if insufficient B is supplied, the catalytic process can use B from the core of a coaxial nanowire and in the process only leave the outer shell thus forming a BO_x nanotube. Our findings provide new insight into the catalytic growth of nanowires and nanotubes. The technique paves the way for a new class of TEM based in situ studies which can be conducted in almost any TEM since no specialized equipment is required. In addition the potential for room temperature growth of nanowires holds promise in various fields, for example, in microelectronics.

■ ASSOCIATED CONTENT

Supporting Information

Still frame movie of the nanowires growth. Laser ablation procedure of the precursor material and other synthesis products. Relation between growth rate and nanowire diameter. EELS studies of the nanowires. Morphological changes of the Au nanoparticles through the growth process. Correlation between the nanoparticle's width and the nanowire's diameter. Variation of the B and O at. % content in the irradiated spot of the precursor material. Formation rate of the nanotubes. EDS of the hybrid nanostructures. Beam-induced material transport. Diagram of activity regimes during the in situ synthesis. Schematic of the Knotek–Feibelman desorption mechanism. Estimations of the beam-induced temperature rise in the Au nanoparticles and in the precursor composite. This material is available free of charge via the Internet at http://pubs.acs.org.

■ AUTHOR INFORMATION

Corresponding Author

*E-mail: mhr1@skku.edu.

Author Contributions

I.G.G.M. and M.H.R. conceived the experiments. The study was managed by M.H.R. I.G.G.M. performed the in situ experiments. I.G.G.M., S.M.G., A.B., and J.Z. contributed to the experiments. All authors participated in the analysis of data and to the writing of the manuscript.

Notes

The authors declare no competing financial interest.

■ ACKNOWLEDGMENTS

I.G.G.M. (DFG RU1540/15-2), V.B., J.K., and G.C. acknowledge financial support from the DFG (project KU 2347/2-2). This work was supported by the Institute of Basic Science (IBS) Korea (EM: 1304). We would like to thank the IFW Dresden and in particular the Institute for Solid State Research (IFF) for granting us use of their microscopy facilities and F.

Boerrnert and G. Kreutzer who are currently responsible for looking after the JEOL 2010F TEM.

■ ABBREVIATIONS

BNW, boron nanowire; NW, nanowire; NP, nanoparticle; CVD, chemical vapor deposition; TEM, transmission electron microscopy(e); EDS, energy dispersive spectra; EFTEM, energy-filtered transmission electron microscopy; EELS, electron energy loss spectroscopy

■ REFERENCES

(1) Orlovskaya, N.; Lugovy, M., Eds. *Boron rich solids: Sensors, ultra high temperature ceramics, thermoelectrics, armor*; NATO Science for Peace and Security Series B: Physics and Biophysics; Springer: New York, 2010.

(2) Cao, L. M.; Zhang, Z.; Wang, W. K. Magnetron sputtering synthesis of large area well-ordered boron nanowire arrays. *Sci. China Ser. G* **2004**, *47*, 403−415.

(3) Cao, L. M.; Zhang, Z.; Sun, L. L.; Gao, C. X.; He, M.; Wang, Y. Q.; Li, Y. C.; Zhang, X. Y.; Li, G.; Zhang, J.; Wang, W. K. Well-aligned boron nanowire arrays. *Adv. Mater.* **2001**, *22*, 1701−1704.

(4) Cao, L. M.; Hahn, K.; Wang, Y. Q.; Scheu, C.; Zhang, Z.; Gao, C. X.; Li, Y. C.; Zhang, X. Y.; Sun, L. L.; Wang, W. K.; Rühle, M. Featherlike boron nanowires arranged in large-scale arrays with multiple nanojunctions. *Adv. Mater.* **2002**, *14*, 1294−1297.

(5) Otten, C. J.; Lourie, O. R.; Yu, M.-F.; Cowley, J. M.; Dyer, M. J.; Ruoff, R. S.; Buhro, W. E. Crystalline boron nanowires. *J. Am. Chem. Soc.* **2002**, *124*, 4564−4565.

(6) Meng, X. M.; Hu, J. Q.; Jiang, J.; Lee, C. S.; Lee, S. T. Boron nanowires synthesized by laser ablation at high temperature. *Chem. Phys. Lett.* **2003**, *370*, 825−828.

(7) Zhang, Y.; Ago, H.; Yumura, M.; Komatsu, T.; Ohshima, S.; Uchida, K.; Iijima, S. Synthesis of crystalline boron nanowires by laser ablation. *Chem. Commun.* **2002**, *23*, 2806−2807.

(8) Li, Z.; Baca, J.; Wu, J. In situ switch of boron nanowire growth mode from vapor-liquid-solid to oxide-assisted growth. *Appl. Phys. Lett.* **2008**, *92*, 113104 ff.

(9) Yang, Q.; Sha, J.; Xu, J.; Ji, Y. J.; Ma, X. Y.; Niu, J. J.; Hua, H. Q.; Yang, D. R. Aligned single crystal boron nanowires. *Chem. Phys. Lett.* **2003**, *379*, 87−90.

(10) Wang, Y. Q.; Duan, X. F. Crystalline boron nanowires. *Appl. Phys. Lett.* **2003**, *82*, 272−274.

(11) Xu, T. T.; Nicholls, A. W.; Ruoff, R. S. Boron nanowires and novel Tube−Catalytic Particle−Wire hybrid boron nanostructures. *Nano* **2006**, *1*, 55−63.

(12) Ross, F. M. Controlling nanowire structures through real time growth studies. *Rep. Prog. Phys.* **2010**, *73*, 114501−114522.

(13) Wu, Y.; Yang, P. Direct observation of Vapor-Liquid-Solid nanowire growth. *J. Am. Chem. Soc.* **2001**, *123*, 3165−3166.

(14) Kodambaka, S.; Tersoff, J.; Reuter, M. C.; Ross, F. M. Germanium nanowire growth below the eutectic temperature. *Science* **2007**, *316*, 729−732.

(15) Gai, P. L.; Sharma, R.; Ross, F. M. Environmental (S)TEM studies of Gas−Liquid−Solid interactions under reaction conditions. *MRS Bull.* **2008**, *33*, 107−114.

(16) Haruta, M.; Yamada, N.; Kobayashi, T.; Iijima, S. Gold catalysts prepared by coprecipitation for low-temperature oxidation of hydrogen and of carbon monoxide. *J. Catal.* **1989**, *115*, 301−309.

(17) Haruta, M. Size and support-dependency in the catalysis of gold. *Catal. Today* **1997**, *36*, 153−166.

(18) Rümmeli, M. H.; Borowiak-Palen, E.; Gemming, T.; Pichler, T.; Knupfer, M.; Kalba, M.; Dunsch, L.; Jost, O.; Silva, S. R. P.; Pompe, W.; Büchner, B. Novel catalysts, room temperature and the importance of oxygen for the synthesis of single-walled carbon nanotubes. *Nano Lett.* **2005**, *5*, 1209−1215.

(19) Uchiyama, T.; Yoshida, H.; Kuwauchi, Y.; Ichikawa, S.; Shimada, S.; Haruta, M.; Takeda, S. Systematic morphology changes of gold nanoparticles supported on CeO_2 during CO oxidation. *Angew. Chem., Int. Ed.* **2011**, *50*, 10157−10160.

(20) Laval, J. Y.; Westmacott, K. H. Electron beam sensitivity and structure of the glassy phase of ceramics. *Inst. Phys. Conf. Ser.* **1980**, *52*, 295−298.

(21) De Natale, J. F.; Howitt, D. G. A mechanism for radiation damage in silicate glasses. *Nucl. Instrum. Methods, B* **1984**, 489−497.

(22) Rogers, J. W., Jr.; Knotek, M. L. The oxidation of polycrystalline Boron: The interpretation of AES and ELS results. *Appl. Surf. Sci.* **1982**, *13*, 352−364.

(23) Knotek, M. L.; Feibelman, P. J. Stability of ionically bonded surfaces in ionizing environments. *Surf. Sci.* **1979**, *90*, 78−90.

(24) Hanke, G.; Müller, K. Low energy Auger transitions in several boron compounds. *J. Vac. Sci. Technol., A* **1984**, *2*, 964−968.

(25) Smith, D. J.; McCartney, M. R.; Bursill, L. A. The electron-beam-induced reduction of transition metal oxide surfaces to metallic lower oxides. *Ultramicroscopy* **1987**, *23*, 299−304.

(26) McCartney, M. R.; Crozier, P. A.; Weiss, J. K; Smith, D. J. Electron-beam-induced reactions at transition metal oxide surfaces. *Vacuum.* **1991**, *42*, 301−308.

(27) Cazaux, J. Correlations between ionization radiation effects in transmission electron. *Ultramicroscopy* **1995**, *60*, 411−425.

(28) Liu, M.; Xu, L.; Lin, X. Heating effect of electron beam bombardment. *Scanning* **1994**, *16*, 1−5.

(29) Egerton, R. F.; Li, P.; Malac, M. Radiation damage in the TEM and SEM. *Micron* **2004**, *35*, 399−409.

(30) Liu, L.-C.; Risbud, S. H. Realtime hotstage highvoltage transmission electron microscopy precipitation of CdS nanocrystals in glasses: Experiment and theoretical analysis. *J. Appl. Phys.* **1994**, *76*, 4576−4580.